Annals of Nuclear Energy 182 (2023) 109590

Contents lists available at ScienceDirect

Annals of Nuclear Energy

journal homepage: www.elsevier.com/locate/anucene

Optimization design of surface microstructure of high-efficiency space radiation heat dissipation fins

Yiqi Zhao [a], Yongnian Song [a], Nailiang Zhuang [a,b,*], Hangbin Zhao [b,c], Xiaobin Tang [a,b]

[a] Department of Nuclear Science and Technology, Nanjing University of Aeronautics and Astronautics, Nanjing 211106, China
[b] Key Laboratory of Nuclear Technology Application and Radiation Protection in Astronautics, Ministry of Industry and Information Technology, Nanjing 211106, China
[c] College of Astronautics, Nanjing University of Aeronautics and Astronautics, Nanjing 211106, China

ARTICLE INFO

Keywords:
Space thermal radiation
Space nuclear reactor
Surface microstructure
Radiation heat flow
Heat conduction

ABSTRACT

With the continuous progress of deep space exploration, the need to develop high-power spacecraft has become urgent. The mass and volume of high-powered spacecraft radiators account for a large percentage. Therefore, an efficient and lightweight space radiation cooling system is one of the key research directions that need to be developed in the future. In the present study, from the perspective of strengthening the radiant heat flow rate unit mass (Φ/m), the improvement idea of adding "triangular rib", "arc rib" and "wave rib" types of surface microstructure on the traditional plate radiation fins is proposed. The heat conduction and the radiation process were simulated by COMSOL Multiphysics®. The effects of parameters, such as microstructure thickness, top angle, heat source spacing and environment temperature on index Φ/m were analyzed. The optimal parameter arrangement of the surface microstructure was obtained, and the mechanism was revealed from the view of thermal conductivity and radiation heat dissipation.

1. Introduction

With the advantages of high output power, large energy density, and long operability, space nuclear power systems (SNPSs) have become among the most promising options for deep space exploration. Most of the heat generated by spacecraft must be dissipated to the space environment through the radiation and heat dissipation system (RHDS). Thus, the mass and volume of the radiator are large (Hyers et al., 2012; Wang et al., 2017). For example, the volume of the RHDS of a SNPS usually occupies approximately 60 % of its volume, directly affecting the overall design layout of the SNPS and the launch weight (El-Genk, 2008; Ma et al., 2021). Therefore, the need to reduce the size and mass of the RHDS by improving its efficiency is urgent.

Given the extremely high vacuum in space, the heat dissipation process of spacecraft in the absence of atmosphere depends mainly on the radiation to the surrounding environment. With the development of thermal control technology, the variety of space radiation radiator designs has become increasingly diverse, such as the conventional pumped fluid loop radiators used in high-power radiators (Ning et al., 2015; Iwata et al., 2021), the liquid metal heat pipe radiator with high heat dissipation efficiency (Wang et al., 2013; Romano and Ribeiro, 2019; Shukla, 2015), and the highly lightweight liquid droplet radiator, which is in the conceptual design stage (Chong et al., 2021; Yang et al., 2021).

Heat pipe is applied to enhance the thermal conductivity of radiators, the thermal properties of heat pipe radiators are also modeled and analyzed to derive optimal design parameters for radiators (Li et al., 2022). Several studies have been conducted to enhance the heat transfer efficiency of radiators. Titanium water heat pipe radiator for kilowatt level waste heat emission was developed and the heat pipe was structurally designed to verify its heat transfer and heat dissipation performance enhancement through testing (Lee et al., 2018, 2020; El-Genk and Tournier, 2011; Hartenstine et al., 2008).

For most radiators, fins are an important medium for heat exchange with the environment. For example, the international space station (ISS) radiator has an unfolded flat fin structure, as shown in Fig. 1(a) (Toughsf, 2017). SNPSs also have large mass and volume. Fig. 1(b) presents the nuclear static thermoelectric reactor (NUSTER) diagram. The cone-shaped structure is the radiator, and the strips that can be expanded in space are the fins (Tang et al., 2020). Under the premise of ensuring that the spacecraft has sufficient heat dissipation area to achieve a certain heat dissipation power, some studies proposed the concept of lightweight radiators to reduce the overall mass and structural dimensions of the radiator (Yan et al., 2022; Tomboulian, 2014; Bieger and Ma, 2011). Some studies have improved on the radiant radiator of TOPAZ-II by using carbon fiber fin material (C—C) for the quality

* Corresponding author at: Department of Nuclear Science and Technology, Nanjing University of Aeronautics and Astronautics, Nanjing 211106, China.
E-mail address: zhuangnailiang@nuaa.edu.cn (N. Zhuang).

https://doi.org/10.1016/j.anucene.2022.109590
Received 7 August 2022; Received in revised form 20 October 2022; Accepted 14 November 2022
Available online 21 November 2022

Nomenclature

General

A	Area (m^2)
W	The width of the fins
L	The heat source spacing (Length) of the fins
m	Mass of the fins
T	Temperature (K)
Q	Heat transfer quantity (J)
Φ	Heat flow rate (W)
q	Heat flow density (W/m^2)
J	Radiosity of the radiator (J)
E	Radiant energy (J)
X	Radiation angle factor
C_0	Blackbody radiation coefficient (W/m^2*K)

Greek

λ	Heat transfer rate (W/m*K)
ε	Emissivity
σ	Blackbody radiation constant

Subscript

S	Surface
amb	Ambient
Shell	Regenerator shell
b	Blackbody

abbreviation

SNPS	Space Nuclear Power Systems
RHDS	Radiation and Heat Dissipation System
ISS	International Space Station
NUSTER	Nuclear Static Thermoelectric Reactor

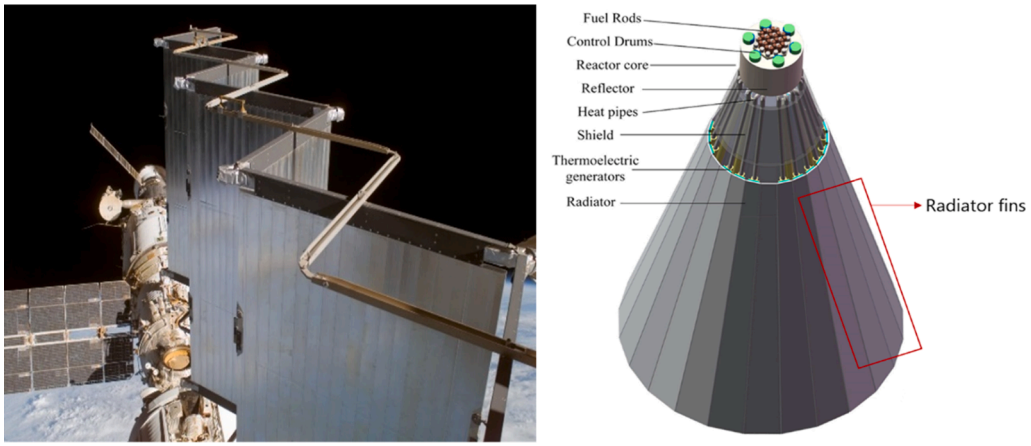

Fig. 1. Structure of the spacecraft's fins. (a) ISS radiator's fins (support spars) (Toughsf, 2017) (b) NUSTER-10's schematic diagram (Tang et al., 2020).

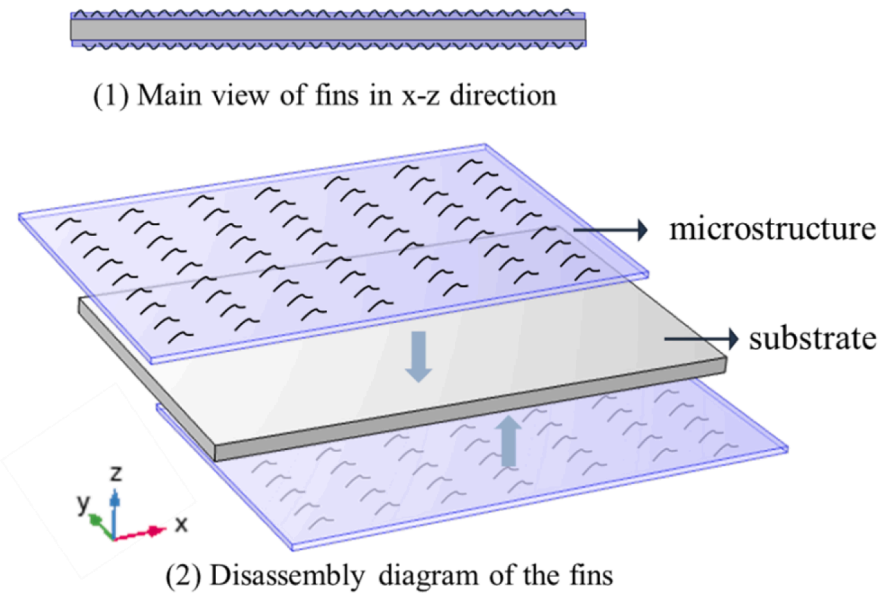

Fig. 2. Microstructure and plate position relationship.

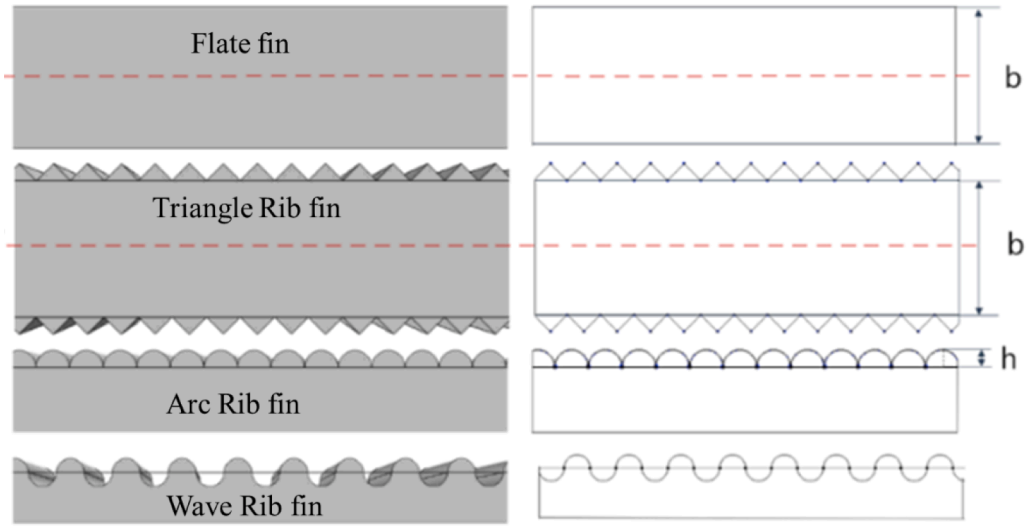

Fig. 3. Three types of microstructures and flat fins.

optimization of the radiator and the improvement of its radiant heat dissipation performance (Habibian et al., 2018; Zhang et al., 2016; Rawal et al., 2005).

For the design of the fin structure, most studies are carried out from convection heat exchangers. The ribs are installed inside the tubes or on the surface of the fins to enhance fluid disturbance and thus strengthen heat transfer. For the compact heat exchanger, the radiation performance is improved by enhancing the heat transfer using the strip fins (Asadi and Khoshkhoo, 2013). For the current space applications of heat exchangers, a study proposed a kind of metal–polymer composite heat exchanger with V-shape microgrooves to improve the space utilization of heat exchangers (Sun et al., 2017), indicating that the special structure of the contact surfaces enhances heat transfer, especially convection heat transfer. Therefore, the effect of different surface structure fins on radiation heat dissipation in space deserves further study.

The present study proposes the idea of using the microstructure to increase the radiant heat flow rate per unit mass (Φ/m) of the fin. Three types of microstructure were proposed and compared. The effects of configuration parameters, such as microstructure height, top angle, heat source spacing, and the environment temperature are analyzed. Furthermore, the calculation results of the optimized fins were compared to evaluate the improvement of the heat dissipation performance of the fins.

2. Simulation method

This section briefly introduces the design and optimization ideas of fin surface microstructure, which are described in terms of fin model construction and the process of mesh model building. The mesh sensitivity analysis and model validation are performed on the fin model.

2.1. Design ideas for surface microstructures

For the structure of the optimized fins. It is assumed that the surface of the conventional radiation fin is a smooth structure (called "substrate"), and two layers of the surface microstructure are added on it. According to the study of v-rib (Williams et al., 2017) (called "triangular rib"), two other kinds of surface microstructure were designed for "arc rib" and "wave rib", and the three structures were compared with the flat fins. The new shapes of microstructure were proposed to further increase the heat exchange area. For some simulations the length and width are variables (the length is determined by the design parameters of the radiator, and the width is determined by the design parameters or the heat conduction tube spacing).

According to Fig. 2, the bottom plate structure is defined as the "substrate" of the heat dissipation fins, that is, the plate structure is used for comparison in the subsequent simulation. A new structure is defined as a "microstructure" (except for the waveform-optimized structure) that is overlaid on the upper and lower surfaces and has the same size as the cross-section in the x–y direction. The integral structure (microstructure and substrate in one piece) is the optimized structure of the radiator fin compared with that of the flat fins. Given the symmetry of the temperature conduction of the fins along the z-direction, half of the fin structure is selected for simulation in this research. Fig. 3 presents the schematic diagram comparing the microstructure and the plate structure. In this study, the surface structure is improved based on the "V-rib (triangular rib)", and the "arc-rib" and "wave-rib" microstructure with large surface areas are proposed. By analyzing the effect of microstructure thickness, the top angle (θ) of the structure (Fig. 4), ambient temperature, the fin width, and the heat source spacing, the parameter "Φ/m" is introduced to evaluate the radiation heat dissipation efficiency

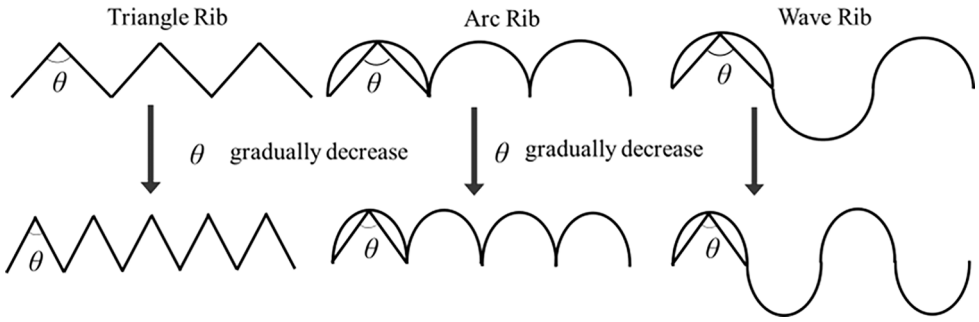

Fig. 4. Definition of the top angle of a structure.

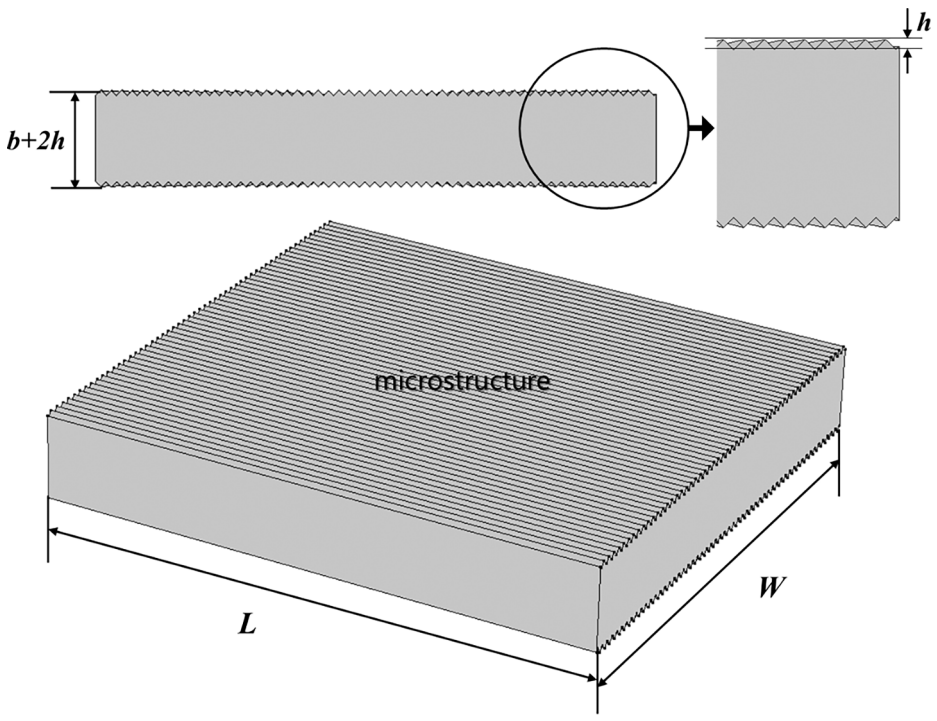

Fig. 5. The overall size and structure diagram of the fin model with triangle ribs.

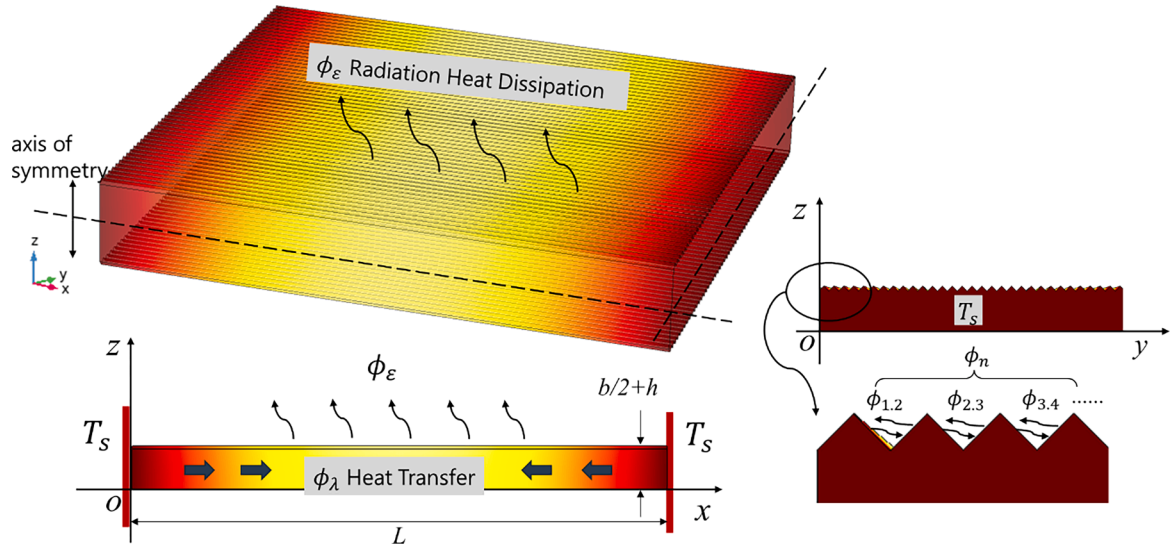

Fig. 6. The heat dissipation fin temperature conduction model.

of the fins, which is then compared to the flat structure to evaluate the improvement in the radiant heat dissipation performance of the fins.

This research simulates and calculates the radiant heat dissipation performance of radiant fins. The overall size and structure diagram of the fin model with triangular ribs as an example are shown in Fig. 5.

2.2. Numerical system and boundary conditions

The heat transfer process of the fin model is divided into two parts. One is the heat conduction process in the fin, the other is the fin surface and space radiation heat dissipation process. Two processes occur simultaneously and the following assumptions should be made:

(1) The radiation heat dissipation of the upper and lower surfaces and internal heat conduction process of the integral fin model are symmetrically distributed, and half of the fin model is selected for simulation.
(2) Heat conduction inside fins is a two-dimensional steady heat conduction process.
(3) The fin model is adiabatic except for the contact surface of the heat source and the microstructure surface.
(4) The fin is made of isotropic material.

The heat conduction process in fins can be regarded as a two-dimensional heat conduction process. The heat dissipation fin temperature conduction model is shown in Fig. 6. Since the fin model is symmetrical along the x-y plane, half of the fin structure is selected for

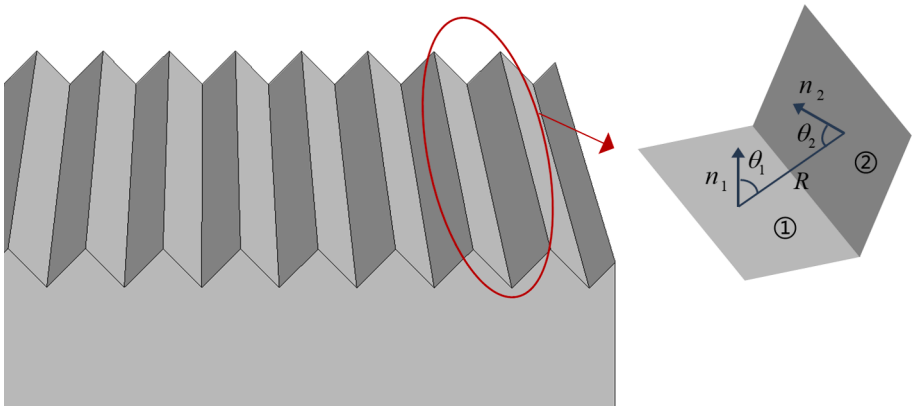

Fig. 7. The triangular fin microstructure schematic diagram.

simulation.

For the two-dimensional steady-state thermal conductivity process, the heat conduction equation and boundary conditions of the fin model heated by a bilateral heat source can be expressed as:

$$T_s|_{x=0,0\leqslant z\leqslant b/2+h} = T_s|_{x=l,0\leqslant z\leqslant b/2+h} = 600K \tag{1}$$

$$\left.\frac{\partial T}{\partial z}\right|_{0\leqslant x\leqslant L,z=0} = 0 \tag{2}$$

$$\left.\frac{\partial T}{\partial x}\right|_{x=L/2,0\leqslant z\leqslant h+b/2} = 0 \tag{3}$$

$$-\lambda A_\lambda \left.\frac{\partial T}{\partial n}\right|_{fin\ \ surface} = \phi_\varepsilon \tag{4}$$

where ϕ_ε is the heat flow radiated from the fin surface to the environment, T_s is the heat source temperature set in simulation., λ is the thermal conductivity of the fin, A_λ is the heat source contact area. The heat source in the simulation is located on the y-z side of the fin, with heat input along the × direction and a known temperature. Radiation boundary conditions are set on the surface of the fin microstructure. The initial temperature of the fin in the simulation is 293.15 K.

Compared with the traditional flat fin, the surface structure of the optimized heat dissipation fin is more complicated. Due to the influence of radiation angle, there will be some heat loss in the process of radiation heat dissipation between the surface and the environment. The effective radiation heat of the fin to the environment can be expressed as

$$\phi_\varepsilon = \phi_a - \phi_n - \phi_s \tag{5}$$

In this formula ϕ_a is the input radiation heat flux, ϕ_n is the radiation heat flux between ribs, ϕ_s is the radiation heat flow of the fin to the environment (without considering the radiation heat flux between surfaces) and it can be calculated as

$$\phi_s = A(1 - X_n)E_b(T_a) \tag{6}$$

$$E_b(T) = n^2\sigma T^4 \tag{7}$$

where A is the area of the fin surface, X_n is the structural surface angle coefficient. $E_b(T)$ is the radiation energy, it's a function affected by temperature. T_a is the ambient temperature, which is set as 3 K. σ is the blackbody radiation constant, which is 5.67 × $10^{-8}m^2{\cdot}K^4$.

Due to the influence of the angle coefficient, the heat radiated from the surface cannot be fully dissipated into the environment. The radiation heat flux received by other surfaces can be expressed as

$$\phi_n = AJX_n \tag{8}$$

J is the radiosity of the radiator, which can be expressed as

$$J = \varepsilon E_b(T) + (1 - \varepsilon)q_a \tag{9}$$

ε is the emissivity of the fin. For the radiation angle coefficient, we take the triangular surface microstructure as an example. A schematic diagram of the triangular fin microstructure is shown in Fig. 7.

Since the surface microstructure can be seen as an array combination of the same structural units, only the angle coefficients of one structural unit need to be calculated. The structural surface angle coefficient X_n can be calculated as

$$X_n = X_{1,2} = \frac{1}{A_1}\int_{A_1}\int_{A_2}\frac{\cos\theta_1\cos\theta_2}{\pi R^2}dA_1dA_2 \tag{10}$$

where $X_{1,2}$ represents the radiation angle coefficient of surfaces 1 and 2. Then ϕ_ε can be expressed as

$$\phi_\varepsilon = A\varepsilon[q_n - E_b(T_A)] \tag{11}$$

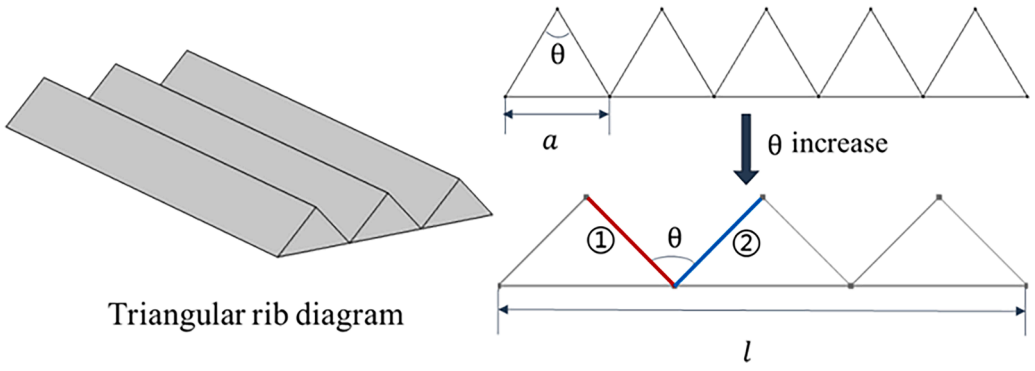

Fig. 8. Schematic diagram of triangular surface microstructure.

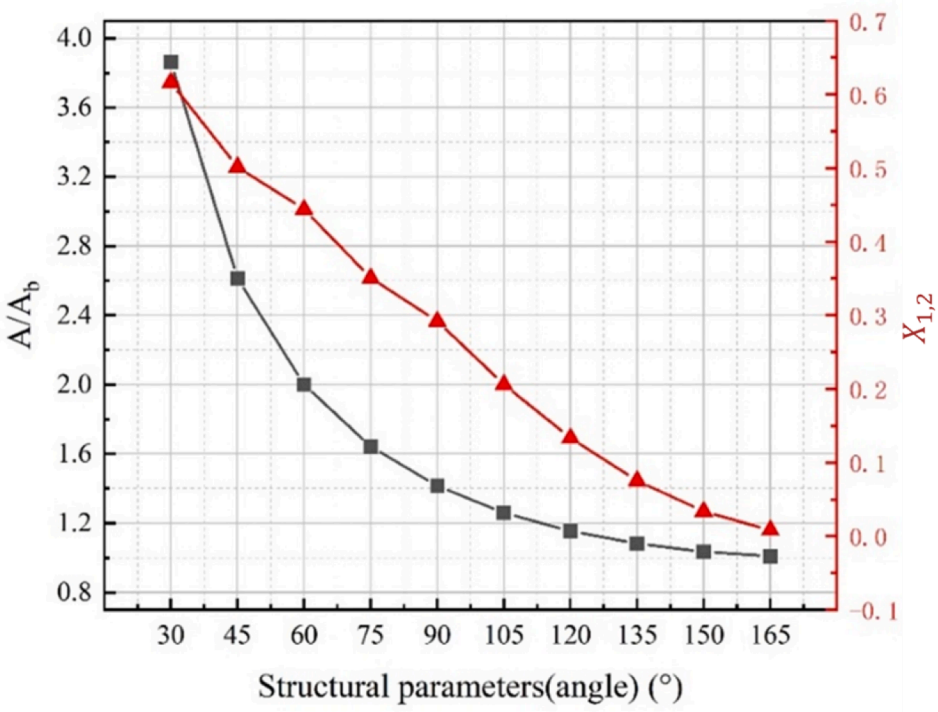

Fig. 9. Variation of radiation angle coefficients and area optimization with the microstructure's top angle.

Table 1
Fin simulation main parameters.

Parameters (unit)	Symbol	Value
Length (Heat source spacing) (mm)	L	–
Width (mm)	W	–-
Substrate thickness(mm)	b	0.4
Microstructure height(mm)	h	–-
Material	–-	C—C
Emissivity	ε	0.85
Thermal conductivity (W/(m·K))	λ	219
Heat source temperature	T_s	600 K
Ambient temperature	T_a	3 K
Initial temperature of the fin	T_0	293.15 K

and the simulation process implemented by COMSOL.

Since the radiation heat dissipation is not simply increasing with the increase of surface area. Take the triangular surface microstructure as an example (as shown in Fig. 8), while introducing A/A_b to denote the surface area of the microstructure on the unit base area.

$$\frac{A}{A_b} = \frac{1}{\sin\frac{\theta}{2}} \tag{12}$$

The variations of radiation angle coefficient $X_{1,2}$ and A/A_b with the increase of the structure's top angle θ are shown in Fig. 9. As can be seen from Fig. 9, the smaller the top angle of the structure θ, the denser the microstructure and the larger the A/A_b., which causes the structure more complex. But at the same time, the more complex the surface structure, the greater the $X_{1,2}$, the radiation loss caused by the angular coefficient. Therefore, a more detailed design and analysis of the structure is needed to improve the radiation heat dissipation efficiency of fins.

Besides, the fins in the simulation are made of lightweight carbon composite materials (C—C fiber), and the thickness of the fin substrate is 0.4 mm according to the design parameters of TOPAZ-II, as shown in Table 1.

Table 2
Mesh parameters.

Meshes	Max unit size	Min unit size	Max unit growth rate	Calculation time (1 mm × 1mmArc ribs)
Mesh 1	0.5	0.07	2	2 s
Mesh 2	0.3	0.054	1.85	5 s
Mesh 3	0.19	0.04	1.7	10 s
Mesh 4	0.15	0.028	1.6	13 s
Mesh 5	0.1	0.018	1.5	22 s
Mesh 6	0.08	0.01	1.45	107 s
Mesh 7	0.06	7E-03	1.42	309 s
Mesh 8	0.055	4E-03	1.4	694 s
Mesh 9	0.04	3E-03	1.37	1542 s
Mesh 10	0.035	1.5E-03	1.35	2874 s
Mesh 11	0.03	8E-04	1.32	–
Mesh 12	0.02	2E-04	1.3	–

2.3. Mesh sensitivity analysis

The substrate and microstructure of the heat dissipation fins are divided into unstructured meshes. Mesh numbers ranging from tens of thousands to millions are used and divided into 12 groups, namely, Mesh 1 to Mesh 12. The mesh parameters are shown in Table 2.

Taking the 90° top angle triangular rib and arc rib microstructure as an example, the fin section grid is shown in Fig. 10. Given that the main measure of fin optimization in this study is the amount of radiative heat dissipation, the main parameter of interest in the gird sensitivity analysis of the model is radiant heat flow rate Φ. Fig. 11 shows the calculated radiant heat flow on the surface of the 90° top angle triangular rib and arc rib microstructure fins for different grid configurations.

The graphs show that for the "triangular rib" and "arc rib" microstructure fins, the increase in the number of meshes does not cause a significant change in the radiant heat flow rate on the surface of the fins in the Mesh 7 to Mesh 12 range. Therefore, considering the calculation time and accuracy, Mesh 7 was selected for the model in this study.

The proposed optimization structures increase the surface area of the

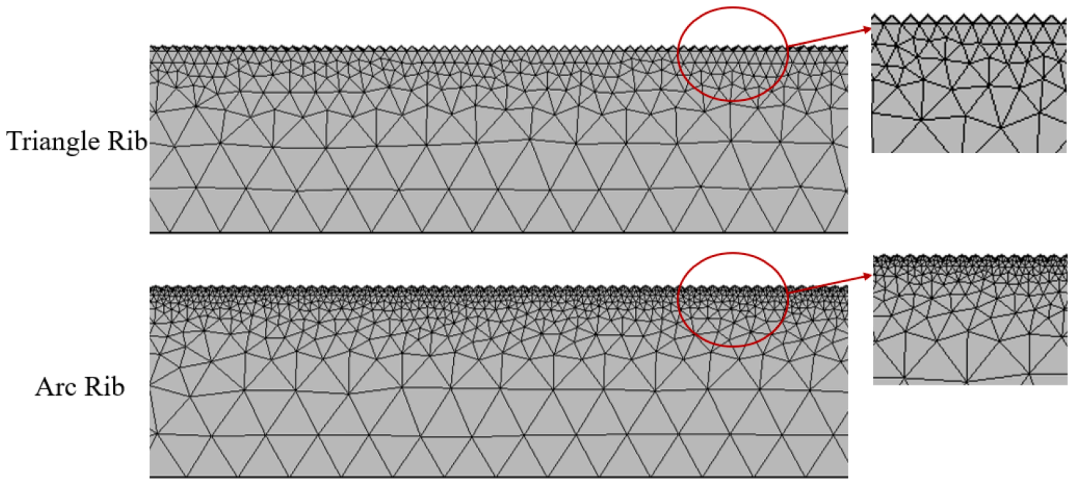

Fig. 10. Detail of fin grid.

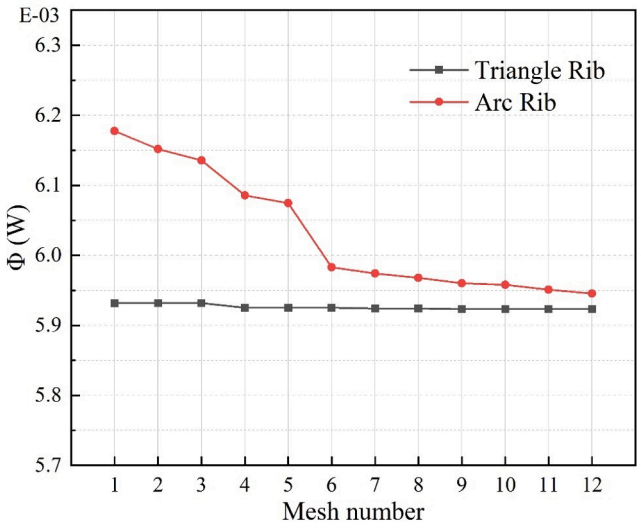

Fig. 11. Grid sensitivity analysis.

fins by increasing the microstructure of the fin surface. Combined with the angle coefficient, the Φ/m of the fins is increased by increasing the effective heat dissipation area of the fins. Considering the lightweight requirement of space radiant radiators, the improvement of the fin dissipation performance is evaluated by the Φ/m. As the increase in microstructure causes an increase in the overall thickness and mass of the fins, the simulation process first studies the optimal thickness range of the fin surface microstructure design. After determining the optimal surface microstructure thickness, the thickness of the microstructure is kept constant, and the size of the three microstructures (top angle or cross-sectional width) is adjusted to select the optimal surface structure. In turn, the length of the fins along the temperature conduction direction is changed, and the change in the radiation heat dissipation rate of each structure is analyzed. Finally, the ambient temperature is adjusted, and the radiation heat dissipation effect is analyzed under the temperature change of radiation heat dissipation fins.

3. Results and discussions

According to the fin model, the radiant heat flow per unit mass (Φ/m) of the fin was simulated and calculated in terms of the microstructure thickness on the fin surface, the microstructure size, the heat source spacing on both sides, the overall width of the fin, and the ambient temperature. Then, the radiation heat dissipation performance of the fins was evaluated.

3.1. Effect of surface microstructure height

The improvement in this study is the addition of a layer of microstructure to the conventional plate-type radiator fins and the increase of the overall quality of the optimized fins. Therefore, the thermal

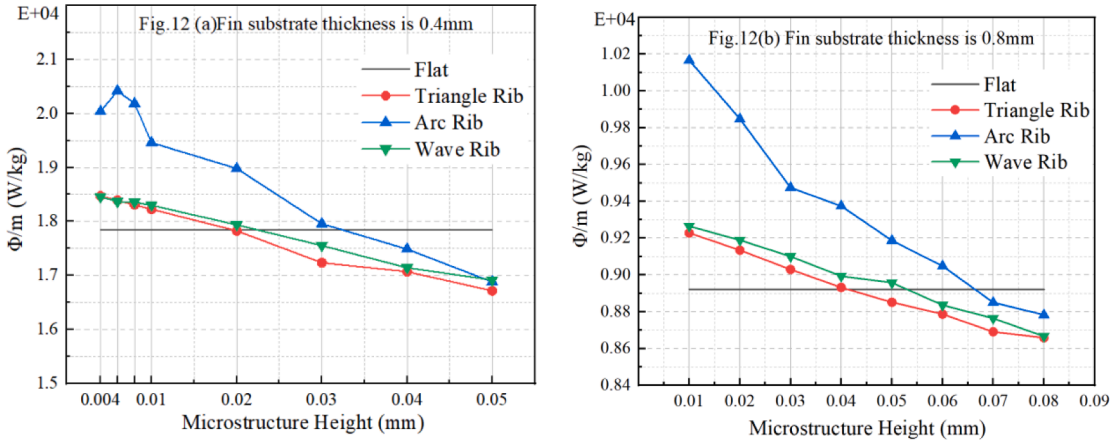

Fig. 12. Trend of Φ/m with microstructure thickness for two kinds of fin substrate thickness.

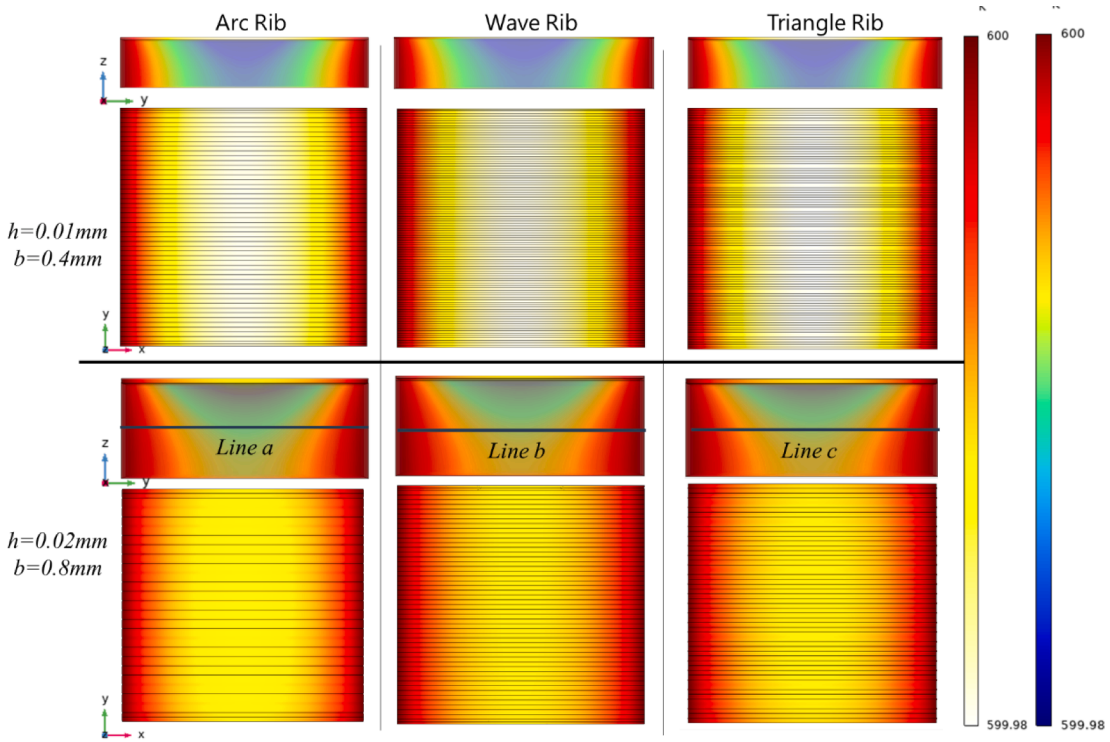

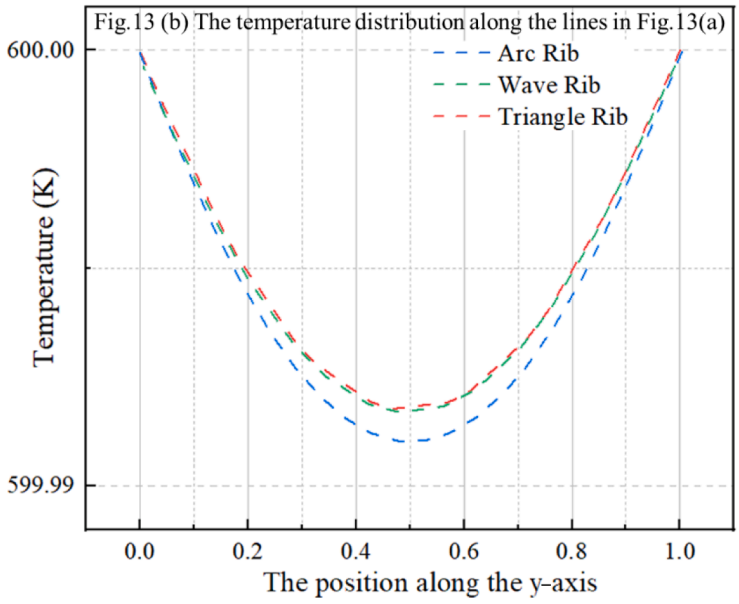

Fig. 13. The fins temperature distribution cloud maps and the temperature distribution along the lines.

performance of the optimized fins is evaluated in combination with the thickness of the microstructure and compared with the thermal efficiency of flat fins. The length and width of the fin model substrate in the simulation are 1 mm, and the top angle of the microstructure is 90°. The size of the microstructure changes with its height. A single-side heat source was set for the fins, and the radiation heat dissipation values per unit mass of the radiator fins with substrate thickness values of 0.4 mm and 0.8 mm were analyzed with the variation of the microstructure height, and the results are shown in Fig. 12.

For the fins with a substrate thickness of 0.4 mm, the thermal performance of the three optimized structure fins is greater than that of the flat plate when the microstructure thickness does not exceed 0.02 mm. For the 0.8-mm substrate, the thickness of the microstructure does not exceed 0.04 mm. Besides, in Fig. 12(a) there is a peak in the range from 0.004 mm to 0.01 mm. That is because when the height of the microstructure decreases, the fin heat dissipation area decreases. The radiation heat loss decreases and the radiation loss caused by the angular coefficient still exists. Therefore, if the microstructure height continues to decrease Φ/m will decrease after reaching the peak. The same rule applies to fins with a substrate thickness of 0.8 mm.

Meanwhile, combined with the temperature distribution cloud map (as shown in Fig. 13), the thinner the fin substrate, the better the fin heat dissipation effect under the same surface microstructure. And in Fig. 13 (a) the lines are chosen from the "$h = 0.02\ mm, b = 0.8\ mm$" fin models to

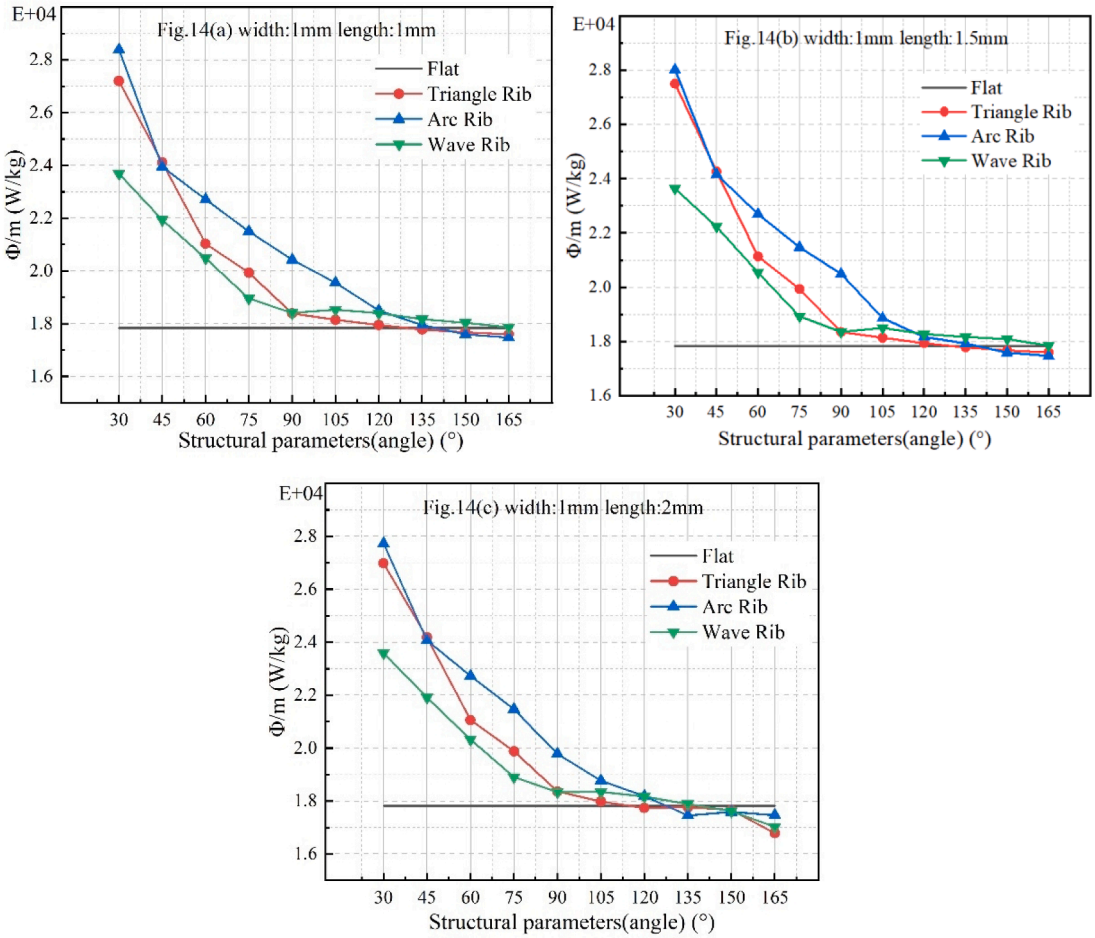

Fig. 14. Trend of three kinds of microstructure and plate Φ/m with angle.

calculate the temperature along the y-axis of the fins. According to the results it can be found that the "arc rib" surface microstructure fins have a best cooling effect than the other microstructure. In terms of overall heat dissipation due to the fact that the microstructure design increases the heat dissipation area to a certain extent. The "arc rib" has a larger surface and cross-section area than the "triangular rib" at the same structural top angle, which affects the overall temperature distribution and the heat dissipation effect. Combined with the fin surface angle coefficient and mass calculation, Φ/m of "arc rib" is larger than that of "triangular rib". The "wave rib" microstructure has a larger surface area than the "triangular rib", but its "concave" structure causes increased radiation heat loss. In turn, the overall mass of the fins continues to increase with the height of the three kinds of microstructure increasing, and the impact on the calculation results continues to increase.

The results of the calculations are summarized as follows. For both 0.4 mm and 0.8-mm substrate thickness values, the three types of fins with microstructures exhibit an improved radiant heat dissipation effect compared to flat fins when the height of the microstructure does not exceed 5 % of the substrate thickness. As the thickness of the surface microstructure increases, the Φ/m of the fins gradually decreases and even drops below the thermal efficiency of the flat plate.

For fins with a substrate thickness of 0.4 mm, the radiant heat flow rate per unit mass of the fins is increased by 14.5 % compared to the flat structure when the microstructure height is 0.006 mm. In the following research, fins with a thickness of 0.4 mm and a microstructure of 0.006 mm were selected for further simulation.

3.2. *Influence of surface microstructure angles*

After identifying the range of microstructures that effectively enhance heat dissipation efficiency, the specific shape and dimensions of the microstructures are analyzed. Given that the thickness of the microstructure is certain when the top angle changes the dimensions, the angular coefficient will change accordingly, which in turn affects the radiant heat flow on the surface of the fin. Meanwhile, the changes in the Φ/m of the fins when the top angles of the three optimized microstructures are in the 30°–165° range and each change of 15° are analyzed. The calculation results are compared with the flat fin to evaluate the heat dissipation performance of the optimized fin. The simulation process starts by heating one side of the fins, keeping the width of the fin constant. The radiation heat dissipation performance of three groups of fins with width-to-length ratios of 1 mm:1 mm, 1 mm:1.5 mm and 1 mm:2 mm are calculated. The variation trend of fin Φ/m with microstructure top angle is shown in Fig. 14.

At the same time, for three kinds of surface microstructure, $\theta = 60°$ and $\theta = 105°$ fin models are selected to analyze the temperature distribution. Fig. 15 shows the temperature of the fins which width-to-heigh ratio is 1 mm: 1.5 mm and the heat source is on one side. Through Fig. 15(a) and Fig. 15(c), it can be seen that when $\theta = 60°$ changes to $\theta = 105°$, the overall temperature of the fin increases and the heat dissipation effect decreases. And according to Fig. 15(b), for the three optimized structures, the temperature of the "arc rib" fins is the lowest and that means "arc rib" fins have the best heat dissipation effect to some extent.

Then, taking the bottom size of 1 mm × 1 mm as an example, the Φ/m values of single-sided and double-sided heating methods are

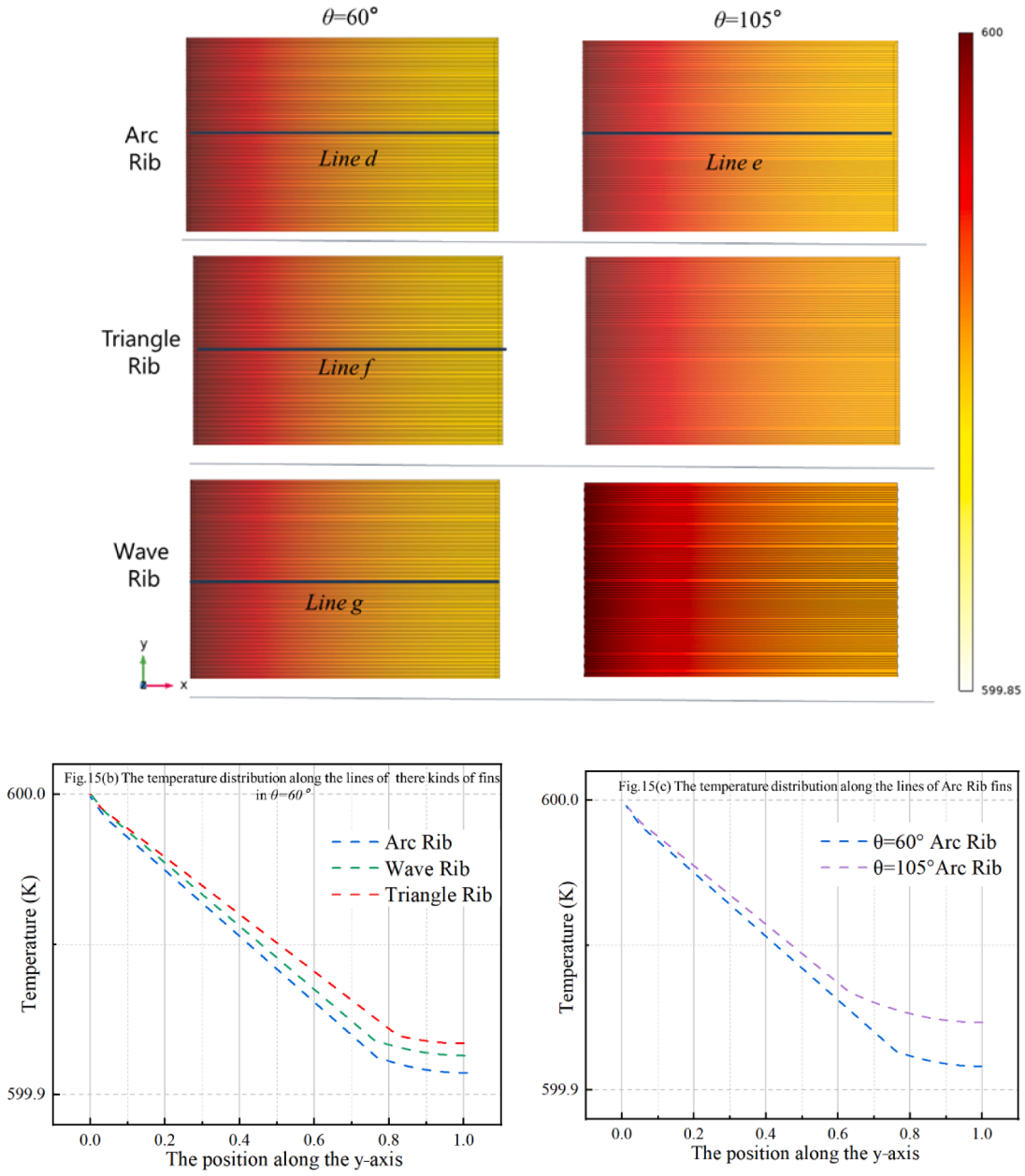

Fig. 15. The temperature distribution diagrams of fins.

compared. As shown in Fig. 16, for fins with the same base area, the Φ/m change trend is basically the same whether the heat source is arranged on one side or both sides.

The increase in microstructure causes an increase in mass compared to flat fins, and the area of radiant heat dissipation decreases as the structure's top angle increases. Fig. 16 shows that the three microstructure fins show a decreasing trend in Φ/m as the top angle increases, eventually converging to or below the flat fins. Given that the mass of the "triangular rib" microstructure does not vary with the top angle, Φ/m decreases at the fastest rate as the radiant heat dissipation area decreases with the increasing top angle of the structure. The "arc rib" has a more effective heat dissipation area than the "triangular rib" and the radiation angle at the same top angle of the structure is less than that of the "wave rib", resulting in the highest Φ/m within a certain range. Among the three microstructures, the "wave rib" fins are lightest in mass, but because of the presence of concave surfaces, the radiation shielding between the surfaces is great, so their advantage is only apparent when the top angle of the structure is large.

In summary, at the structural top angle of 90°, the difference in radiant heat dissipation per unit mass is greater for the "arc rib" fins than that for the triangular and wave fins, with a Φ/m improvement of approximately 11 %. Compared to the flat radiator, the Φ/m of the fins is enhanced by 14.4 %. Considering the fin preparation process, when the microstructure thickness is constant, the width of the individual microstructure decreases with the decrease of θ, but the preparation complexity of the structure and the preparation accuracy are required to increase. In this research, the top angle of the structure is set to be 90° arc rib for the next simulation study.

3.3. *Influence of fin width and heat source spacing*

After determining the shape and size of the microstructure, the practical application of fins with increased microstructure is considered, that is, the waste heat conduction through a heat source (heat pipe or thermal fluid circuit) to the radiator fins. Different design parameters of heat source spacing for radiators with different structures. In the present

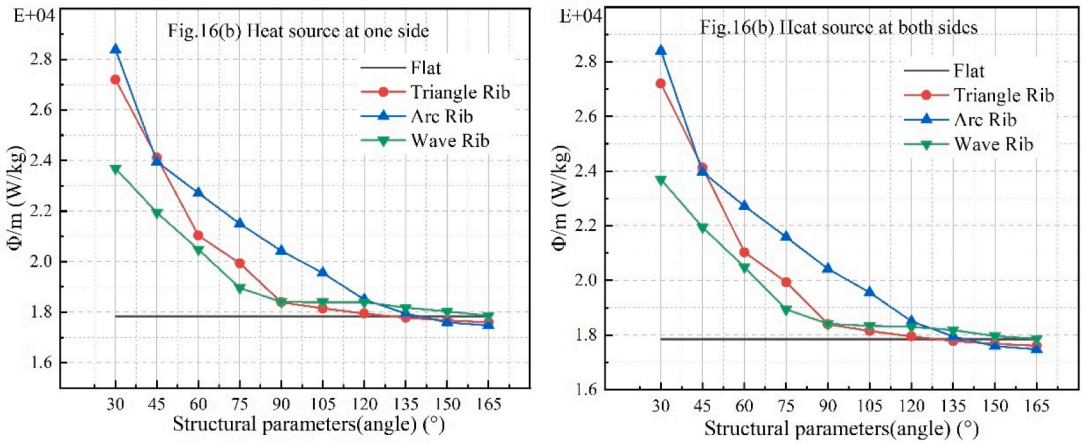

Fig. 16. Heat source arrangement on one or both sides of the Φ/m variation.

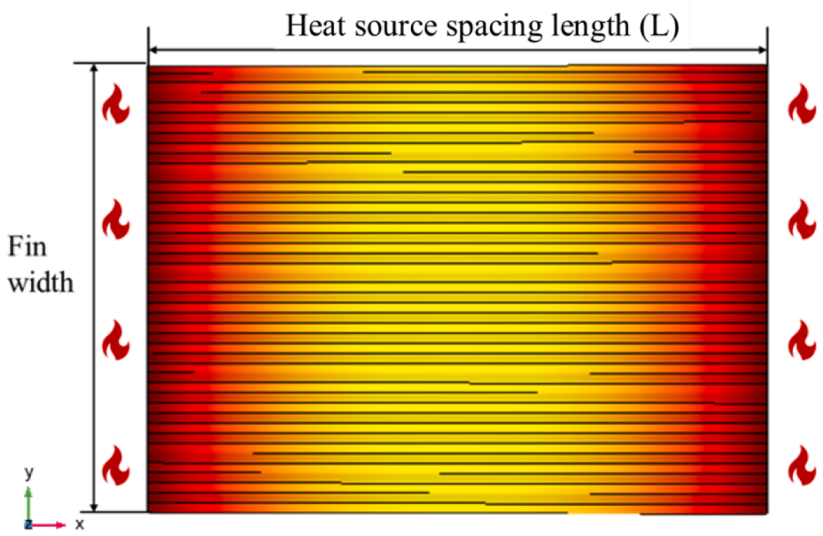

Fig. 17. Top view of fins.

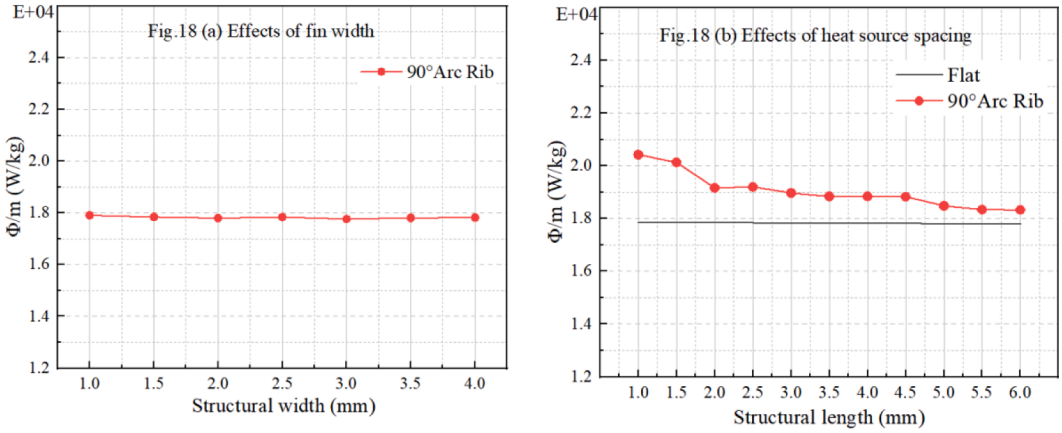

Fig. 18. Effect of fin width and heat source spacing on Φ/m.

study, we take the two-end heating type as an example. When the heat source spacing L is constant, the variation of Φ/m with the increase of width W is calculated, and the schematic diagram is shown in Fig. 17. In turn, the variation of Φ/m with increasing L is simulated for fins of unit width, and the results are shown in Fig. 18. The surface microstructure with a thickness of 0.006 mm is selected, and the substrate thickness is 0.4 mm.

The calculation results show that Φ/m does not change significantly when the heat source spacing of the microstructure is certain, and the width is 1–4 times of the length. Given that the contact temperature heat

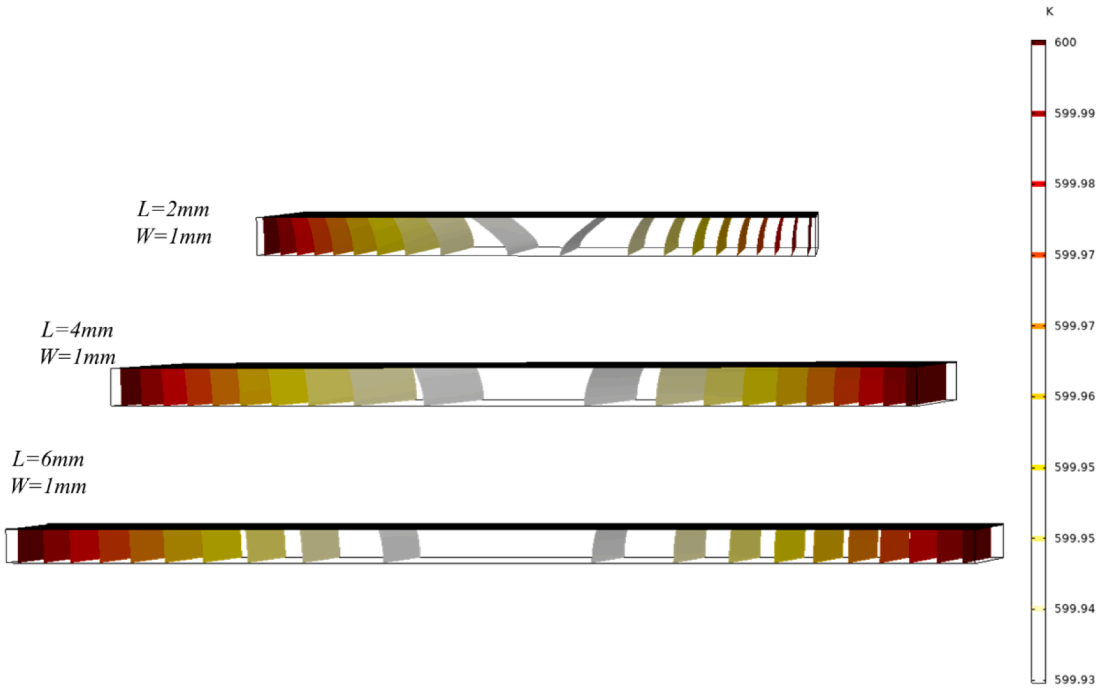

Fig. 19. Fin isotherm distribution of different heat source spacing length.

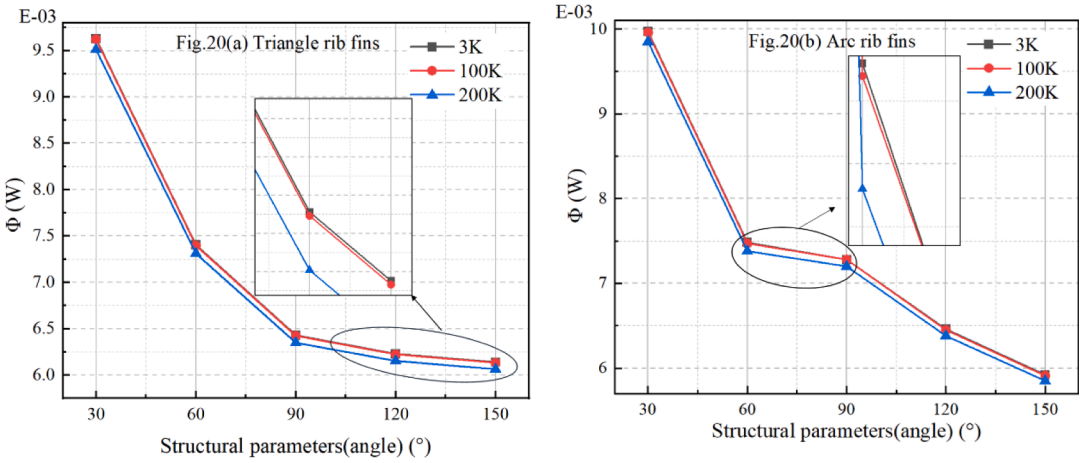

Fig. 20. *Φ/m* of fins at different ambient temperatures.

source of 600 K is targeted along the side of the fins, the temperature distribution of the fins along the width direction will show a certain uniformity, and the radiation heat dissipation capacity will be approximately the same.

When the fin width is constant and the heat source spacing is set to be 1–6 times the width, the radiation heat of the unit mass fin gradually decreases with the increase of the structural heat source spacing. It can be seen from Fig. 19, isotherm distribution that the temperature distribution inside the fin is uniform, and the radiation heat dissipation performance is improved due to the influence of the temperature conduction process at a short heat source spacing. And the temperature of the fins' surfaces decreases more with the decrease of the heat source spacing. The larger the aspect ratio, the closer the thermal performance of the microstructure is to the flat fin.

3.4. Influence of ambient temperature

The ambient temperature affects the effectiveness of the heat dissipation process. The average temperature in space is approximately minus 270 °C, which is equivalent to 3 K, whereas the temperature of the planet's surface varies considerably from day to night. In the case of the Moon, the temperature difference between day and night can exceed 200 °C depending on the position of the Sun's irradiation (Smirnov et al., 2021). In the following simulation, we take the arc and triangular rib fins as an example and analyze the trend of the radiation heat flow of the fins with different structural top angles at 3 K, 100 K, and 200 K ambient temperatures. The calculated results are shown in Fig. 20.

The calculation results show that the two kinds of fins have the same trend of radiant heat flow Φ at different ambient temperatures with different structural top angles. As the temperature of the fins is higher than the ambient temperature during the simulation, the temperature difference between the fins and the ambient decreases when the ambient temperature increases. According to the formula for calculating the radiation heat dissipation, the temperature of the heat end of the fin is fixed, and the difference with the ambient temperature gradually decreases with the increase of the ambient temperature, and the rate of

decrease gradually increases. Therefore, the heat dissipation of the fins decreases when the ambient temperature increases, and the trend of heat dissipation with the size of the structure is constant.

4. Conclusions

The present study proposes to add "surface microstructures" on the top and bottom sides of conventional flat fins to improve the radiant heat flow per unit mass. The effect of structural parameters, such as the thickness of the fin microstructure, the top angle of the microstructure, and the heat source spacing and width, are simulated, and the following conclusions are drawn:

(1) With a microstructure thickness to fin substrate thickness ratio range of 0–1/20, the radiative heat dissipation per unit mass of the optimized fin is greater than that of the flat plate structure. Using the fin microstructure with a substrate thickness ratio of 1.5 % as an example, the effect of different structures on heat dissipation efficiency is analyzed by introducing the "top angle of the structure". The overall thermal performance of the curved microstructure with a top angle of 90° per unit bottom area was found to be the best, with a maximum Φ/m improvement of 61 % compared to the flat structure.
(2) During the operation of the fins, which simultaneously conduct and dissipate heat, the heat dissipation performance gradually approaches that of the flat fins as the heat source spacing increases but is unaffected by the width of the fins.
(3) The ambient temperature does not affect the trend of radiation heat dissipation of different microstructure fins with structural shape and size changes but affects the overall heat dissipation of fins.

In the present study, the fin structure is optimized and can be applied to the radiation cooling system to further analyze the heat dissipation performance of the radiator in the entire operation.

CRediT authorship contribution statement

Yiqi Zhao: Conceptualization, Methodology, Formal analysis, Data curation, Writing – original draft, Writing – review & editing. **Yongnian Song:** Validation, Formal analysis, Data curation. **Nailiang Zhuang:** Resources, Data curation, Supervision, Funding acquisition. **Hangbin Zhao:** Supervision. **Xiaobin Tang:** Supervision, Data curation.

Declaration of Competing Interest

The authors declare that they have no known competing financial interests or personal relationships that could have appeared to influence the work reported in this paper.

Data availability

Data will be made available on request.

Acknowledgment

This work was supported by the National Natural Science Foundation of China (Grant No. 12105142) and the Postgraduate Research & Practice Innovation Program of Jiangsu Province (Grant No. 2021K387C).

References

Asadi, M., Khoshkhoo, R.H., 2013. Investigation into radiation of a plate-fin heat exchanger with strip fins. Mechan. Eng. Res. 5, 82–89. https://doi.org/10.5897/JMER12.059.
Bieger, V., Ma, J., 2011. Investigation of Lightweight Space Radiator Design for Low and No Gravity Environments, in: ASME 2011 Int. Mechan. Eng. Congress and Exposition, IMECE 2011. pp. 1129–1138. Doi: 10.1115/IMECE2011-64646.
Chong, D., Zhu, M., Zhao, Q., Chen, W., Yan, J., 2021. A review on thermal design of liquid droplet radiator system. J. Thermal Sci. 30, 394–417. https://doi.org/10.1007/s11630-021-1419-2.
El-Genk, M.S., 2008. Space nuclear reactor power system concepts with static and dynamic energy conversion. Energ. Conver. Manage. 49, 402–411. https://doi.org/10.1016/j.enconman.2007.10.014.
El-Genk, M., Tournier, J.-M., 2011. Uses of liquid-metal and water heat pipes in space reactor power systems. Front. Heat Pipes 2. https://doi.org/10.5098/fhp.v2.1.3002.
Habibian, S.H., Abolmaali, A.M., Afshin, H., 2018. Numerical investigation of the effects of fin shape, antifreeze and nanoparticles on the performance of compact finned-tube heat exchangers for automobile radiator. Appl. Therm. Eng. 133, 248–260. https://doi.org/10.1016/j.applthermaleng.2018.01.032.
Hartenstine, J., Anderson, W., Bonner III, R., 2008. Titanium Loop Heat Pipes for Space Nuclear Power Systems. AIP Conf. Proc. 969, 44. https://doi.org/10.1063/1.2845001.
Hyers, R.W., Tomboulian, B.N., Craven, P., Rogers, J., 2012. Lightweight, High-Temperature Radiator for Space Propulsion. University of Massachusetts, Huntsville, AL.
Iwata, N., Nakanoya, S., Nobuyuki Miyai, R.N., Takeda, N., Tsutsui, F., 2021. Thermal Performance Evaluation of Space Radiator for Single-Phase Mechanically Pumped Fluid Loop. J. Spacecr. Rockets. doi 10 (2514/1), A35030.
Lee, K.-L., Anderson, W., Tarau, C., 2018. Titanium-Water Heat Pipe Radiators for Kilopower System Cooling Applications. https://doi.org/10.2514/6.2018-4581.
Lee, K.-L., Tarau, C., Anderson, W., Beard, D., 2020. Titanium-Water Heat Pipe Radiators for Space Fission Power System Thermal Management. Micrograv. – Sci. Technol. 32 https://doi.org/10.1007/s12217-020-09780-5.
Li, Z., Zhang, H., Huang, Z., Zhang, D., Wang, H., 2022. Characteristics and optimation of heat pipe radiator for space nuclear propulsion spacecraft. Prog. Nucl. Energy 150, 104307. https://doi.org/10.1016/j.pnucene.2022.104307.
Ma, W., Ye, P., Zhao, G., Yang, X., Wang, J., 2021. Effect of cooling schemes on performance of MW-class space nuclear closed Brayton cycle. Ann. Nucl. Energy 162, 108485. https://doi.org/10.1016/j.anucene.2021.108485.
Ning, X., Wang, Y., Zhang, J., Liu, D., 2015. An equivalent ground thermal test method for single-phase fluid loop space radiator. Chin. J. Aeronaut. 28, 86–92. https://doi.org/10.1016/j.cja.2014.12.011.
Rawal, S., Johnson, K., Makowski, K., 2005. Multifunctional Carbon-Carbon Foam-Core Space Radiator Development 746. Doi: 10.1063/1.1867112.
Romano, L.F.R., Ribeiro, G.B., 2019. Parametric evaluation of a heat pipe-radiator assembly for nuclear space power systems. Therm. Sci. Eng. Progr. 13, 100368 https://doi.org/10.1016/j.tsep.2019.100368.
Shukla, K., 2015. Heat Pipe for Aerospace Applications—An Overview. J. Electron. Cool. Thermal Cont. 05, 1–14. https://doi.org/10.4236/jectc.2015.51001.
Smirnov, S.V., Sinkevich, M.V., Antipov, Y.A., Khalife, H.S., 2021. A calculation method of a heat rejection system in a lunar power plant consisting of a free-piston Stirling engine (FPSE). Acta Astronaut. 180, 46–57. https://doi.org/10.1016/j.actaastro.2020.12.008.
Sun, J., Zhuang, J., Jiang, H., Huang, Y., Zheng, X., Liu, Y., Wu, D., 2017. Thermal dissipation performance of metal-polymer composite heat exchanger with V-shape microgrooves: A numerical and experimental study. Appl. Therm. Eng. 121, 492–500. https://doi.org/10.1016/j.applthermaleng.2017.04.104.
Tang, S., Wang, C., Liu, X., Tian, Z., Su, G., Tian, X., Qiu, S.Z., 2020. Experimental investigations on start-up performance of static nuclear reactor thermal prototype. Int. J. Energy Res. 44 https://doi.org/10.1002/er.5134.
Tomboulian, B.N., 2014. Lightweight, High-Temperature Radiator for In-Space Nuclear-Electric Power and Propulsion (Doctoral Dissertations). University of Massachusetts Amhers.
Toughsf, 2017. All-radiators. URL http://toughsf.blogspot.com/2017/07/all-radiators.htm.
Wang, C., Chen, J., Qiu, S., Tian, W., Zhang, D., Su, G.H., 2017. Performance analysis of heat pipe radiator unit for space nuclear power reactor. Ann. Nucl. Energy 103, 74–84. https://doi.org/10.1016/j.anucene.2017.01.015.
Wang, Jin, Li, Y., Wang, Jun, 2013. Transient performance and intelligent combination control of a novel spray cooling loop system. Chin. J. Aeronaut. 26, 1173–1181. https://doi.org/10.1016/j.cja.2013.07.048.
Williams, J.-P., Paige, D.A., Greenhagen, B.T., Sefton-Nash, E., 2017. The global surface temperatures of the Moon as measured by the Diviner Lunar Radiometer Experiment. Icarus 283, 300–325. https://doi.org/10.1016/j.icarus.2016.08.012.
Yan, L., Dong, Z., Zhang, S., 2022. Thermal Analysis of a Novel Linear Oscillating Machine Based on Direct Oil-Cooling Windings. IEEE Trans. Energy Convers. 37, 1042–1051. https://doi.org/10.1109/TEC.2021.3118930.
Yang, L., Wang, C., Qin, H., Zhang, D., Tian, W., Su, G.H., Qiu, S., 2021. Operation performance analysis of a liquid metal droplet radiator for space nuclear reactor. Ann. Nucl. Energy 158, 108301. https://doi.org/10.1016/j.anucene.2021.108301.
Zhang, W., Ma, Z., Zhang, D., Tian, W., Qiu, S., Su, G.H., 2016. Transient thermal–hydraulic analysis of a space thermionic reactor. Ann. Nucl. Energy 89, 38–49. https://doi.org/10.1016/j.anucene.2015.10.035.